

# Improvement of Light Collection Efficiency of Lens-Coupled YAG Screen TV System for a High-Voltage Electron Microscope

KAZUO YAMAMOTO,<sup>1\*</sup> TAKAYOSHI TANJI,<sup>2</sup> MICHIO HIBINO,<sup>2</sup> PETER SCHAUER,<sup>3</sup> AND RUDOLF AUTRATA<sup>3</sup>

<sup>1</sup>Department of Electronics, Nagoya University, Furo-cho, Chikusa-ku, Nagoya 464-8603, Japan

<sup>2</sup>Center for Integrated Research in Science and Engineering, Nagoya University, Furo-cho, Chikusa-ku, Nagoya 464-8603, Japan

<sup>3</sup>Institute of Scientific Instruments, Academy of Science of Czech Republic, 612 64 Brno, Czech Republic

**KEY WORDS** YAG + glass hemisphere + lens coupling method; high-voltage electron microscope TV system; light collection

**ABSTRACT** A new lens coupling television (TV) system using a YAG (Yttrium Aluminum Garnet:  $Y_3Al_5O_{12} : Ce^{3+}$ ) single crystal screen has been developed for a high-voltage electron microscope (HVEM), and its performance is examined. The system, using a combination of YAG and lenses, is less damaged by high-energy electron irradiation and reduces the influence of X-rays on the image. YAG screens have not been used for lens-coupling systems, because the high refractive index ( $n = 1.84$ ) of YAG results in a low light collection efficiency for emitted light. This disadvantage is overcome by combining a thin YAG disk screen (thickness; 100  $\mu\text{m}$ ) with a glass hemisphere whose refractive index is 1.81. We found that the light intensity is almost the same as that obtained with a conventional P22 powder screen and lenses system. The resolution is about 55  $\mu\text{m}$  on the YAG screen, and this value is 1.3 times higher than that measured by the conventional system. Shading and distortion do not affect TV observation. Detection quantum efficiency, obtained after correction of the channel mixing effect, is about 0.1. *Microsc. Res. Tech.* 49:596–604, 2000. © 2000 Wiley-Liss, Inc.

## INTRODUCTION

As recording devices for a transmission electron microscope (TEM), photographic film, imaging plates (Ayato et al., 1990; Mori et al., 1990), TV cameras, and slow-scan CCD (charge coupled device) cameras (Barbe, 1980; Krivanek and Mooney, 1993) have generally been used in many studies. The TV camera is an especially influential device because it is useful for dynamic observation to clarify physical phenomena. Moreover, it is useful in focusing images, correcting astigmatism, and so forth. The TV system consists of two processes: converting electrons to photons in a scintillation screen, and transferring photons to TV tubes or CCDs. So far, two types of coupling methods have generally been used for the electron microscope TV system. One is a lens coupling (LC) method using a fluorescent powder screen and a transfer lens system (Fan and Ellisman, 1993; Mooney et al., 1994), and the other is an optical fiber coupling (OFC) method using a YAG single crystal screen and an optical fiber plate (Daberko et al., 1991; Krivanek and Mooney, 1993; Weickenmeier et al., 1995). However, there are a number of problems in utilizing these TV systems for high-voltage electron microscopes (HVEMs). The powder screen of the LC method and the optical fiber of the OFC method are damaged by high-energy electron irradiation. Moreover, the influence of X-rays (emitted in the screen) on the image is serious in the OFC method because the distance between the screen and the TV tube is very short compared to the LC method.

We developed a new LC method using the YAG disk screen. The YAG disk screen has not been used with

the LC method because its luminous efficiency is lower than that of the powder screen and its emitted light diverges at the exit surface of the disk because of YAG's high refractive index ( $n = 1.84$ ) (Autrata et al., 1983), resulting in reduced light collection efficiency. The new system, consisting of a thin YAG disk and a glass hemisphere, has been developed to avoid the effect of the high refractive index of YAG.

In this paper, the design and the construction of this new system will be introduced and its performance will be evaluated for the following aspects: (1) Resolution, (2) Light intensity, (3) Shading, (4) Distortion, and (5) Detection quantum efficiency (DQE). The results will also be compared with those of a P22 fluorescent powder screen.

## DESIGN AND CONSTRUCTION

One of the most important points for the YAG and LC TV system is its light collection efficiency. As shown in Figure 1a, the emitted light in the YAG disk is refracted at the exit surface of the disk, so that the maximum angle ( $\theta_1$ ) collecting the light of the lens system reduces to  $\theta_1/1.84$ . If the YAG disk is combined with a glass hemisphere whose refractive index is the same as the YAG, as shown in Figure 1b, the refraction of the light is avoided. Consequently, the image intensity obtained with the YAG disk and glass hemisphere

\*Correspondence to: Kazuo Yamamoto, Department of Electronics, Nagoya University, Furo-cho, Chikusa-ku, Nagoya 464 8603 Japan.  
E-mail: h973203d@mbox.media.nagoya-u.ac.jp

Received: 1 September 1999; accepted in revised form 23 February 2000

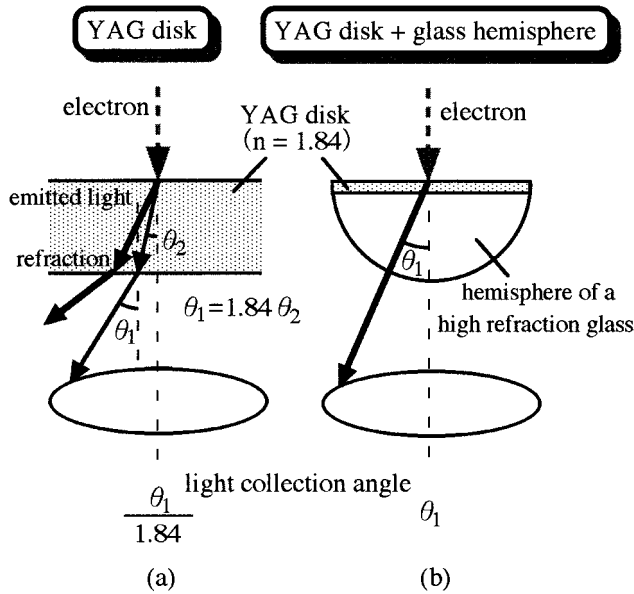


Fig. 1. Light collecting angle of (a) YAG disk + LC system and (b) YAG disk + glass hemisphere + LC system. The angle  $\theta_1$  is the maximum at which a lens system can collect emitted light. The light collection angle of the YAG disk + LC system is  $\theta_1/1.84$ , because of the refraction at the exit surface of the disk. The hemisphere of the high-refraction glass increases the light collection angle.

is 3.4 ( $\approx 1.84^2$ ) times higher than that obtained with the YAG disk alone.

The new TV system constructed for HVEM is shown in Figure 2. A YAG disk with a thickness of 100  $\mu\text{m}$  was placed on a glass hemisphere with a radius of curvature of 53 mm. Aluminum was evaporated to a thickness of 100 nm on the top surface of the YAG disk. The special glass hemisphere was made by combining a cylinder glass with a flat-convex lens. The refractive index of the glass hemisphere was  $n = 1.81$  (SFL6). A light image converted from a 1,000-keV electron image in the YAG disk was transferred to a photocathode of a TV camera through two optical lenses ( $F = 1.2$ ,  $f = 50$  mm and  $F = 1.0$ ,  $f = 50$  mm). The pair of lenses were used to control the magnification of the light image on the photocathode. The TV camera was a Hamamatsu Photonics C-1000 type 12 Silicon intensifier tube (SIT); the resolution, determined by the width of scanning lines, was 40  $\mu\text{m}$  on the photocathode. In this lens system, the glass hemisphere makes a virtual image of the light on the YAG disk plane at a magnification of 1.8. The pair of lenses reduces the image to proper size, and forms the image magnified by a factor of 1.35 on the photocathode. The light collection angle of the system is about  $10^\circ$ . The size of the TV frame that we could observe corresponds to an area  $5.6 \times 4.2$  mm on the YAG disk plane. Since the light emits from almost the center of the flat surface of the glass hemisphere, we could ignore spherical aberration, astigmatism, and coma of the glass hemisphere. Figure 3 shows an illustration of the lens system. The distance between the YAG disk and the photocathode is very long, about 460 mm, compared to the YAG and OFC method (in which it is less than 10 mm), so that the influence of X-rays

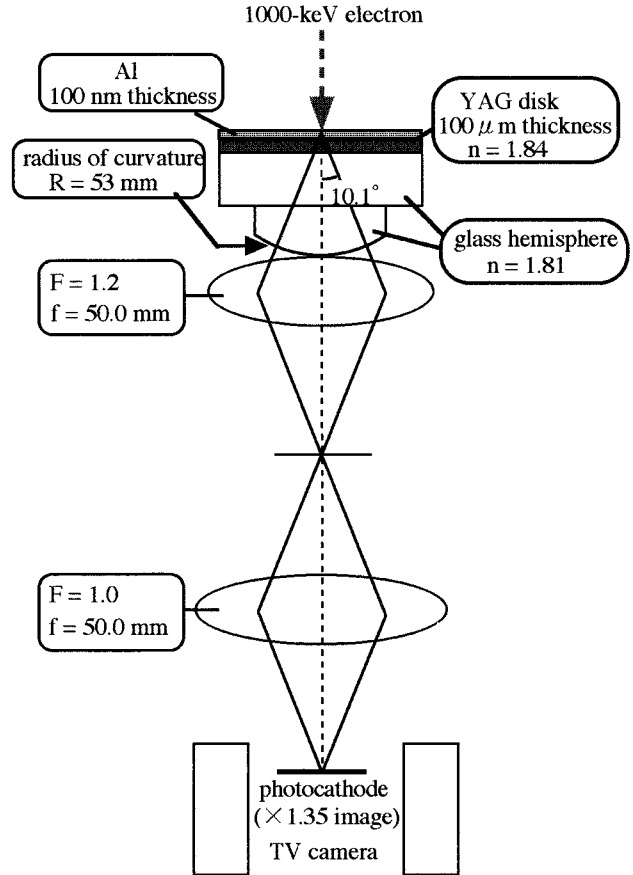


Fig. 2. New LC TV system using the YAG disk and the glass hemisphere. Combining a cylinder glass with a flat-convex lens makes the glass hemisphere.

reduces to less than  $1/2,100$  ( $\approx 1/46^2$ ) that of the YAG and OFC method. An outer view of the new TV system is shown in Figure 4.

**EXPERIMENT AND DISCUSSION**

**Resolution**

The deterioration of the resolution in the new TV system was mainly caused by (1) the electron beam spread in the YAG disk screen, (2) the curvature of image field due to the glass hemisphere, and (3) the misalignment of the lens system. The influence of (2) and (3) was analyzed light-optically without the YAG disk. Figure 5a shows the setup of the light-optical experiment. In order to reproduce the same situation as that of the YAG screen, in which the light emits radiantly, we set a ground glass plate over the new system and introduced a light emitted in a fluorescent screen mounted on a 200-kV TEM (Hitachi H-8000; the wavelength of the light was almost the same as that of the light emitted in YAG). A small knife was put on the glass hemisphere. The resolution was measured as the 20–80% width of the output profile of a small knife edge image. Figure 6 shows the resolution as a function of distance from the center of the flat surface of the glass hemisphere. The curving solid line indicates the

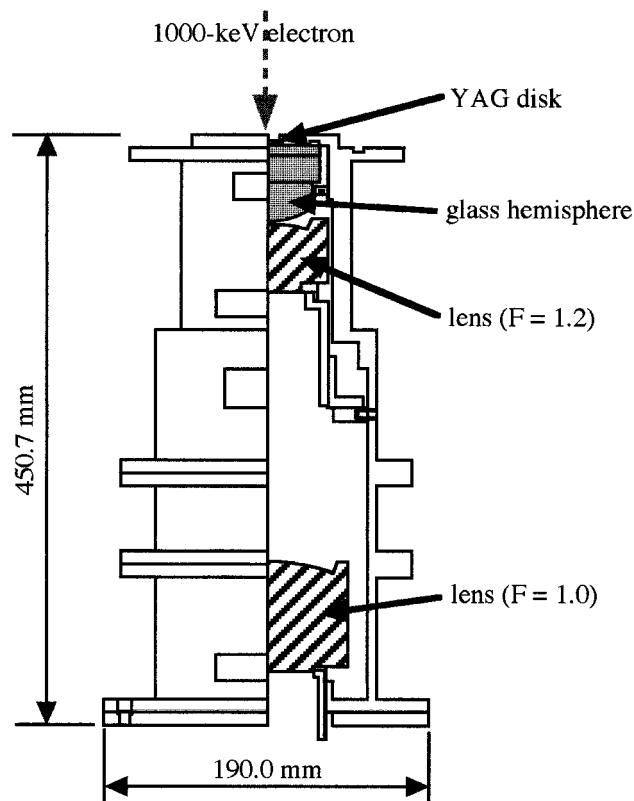


Fig. 3. Illustration of the YAG disk + glass hemisphere + LC system. Since the distance between the YAG disk and the photocathode is more than 46 times that of the YAG + OFC TV system, the influence of X-rays reduces to less than  $1/46^2$ .

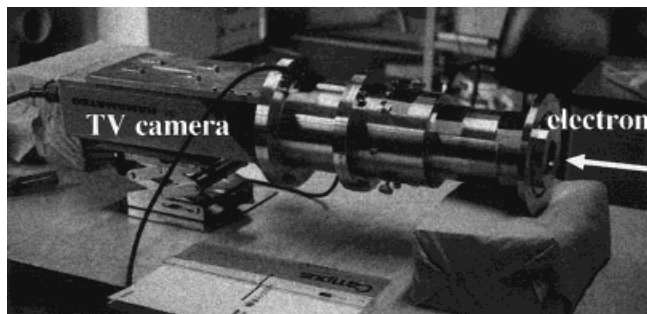


Fig. 4. Outer view of the new TV system.

resolution calculated from a ray-tracing simulation in which the lens system was focused on the flat surface of the glass hemisphere. The image blurred at the corner of the TV monitor view on account of the curvature of the image field. However, when proper defocusing was introduced, the resolution was almost uniform within the area of the TV monitor view and it was 40 to 50  $\mu\text{m}$  on the flat surface of the glass hemisphere. The influence of the misalignment of the lens system was evaluated from the difference between the calculated and measured resolution at the center, and was found to be about 35  $\mu\text{m}$ . Therefore, the influence of the curvature of the image field is estimated to be 30  $\mu\text{m}$  ( $\approx \sqrt{45^2 - 35^2}$ ).

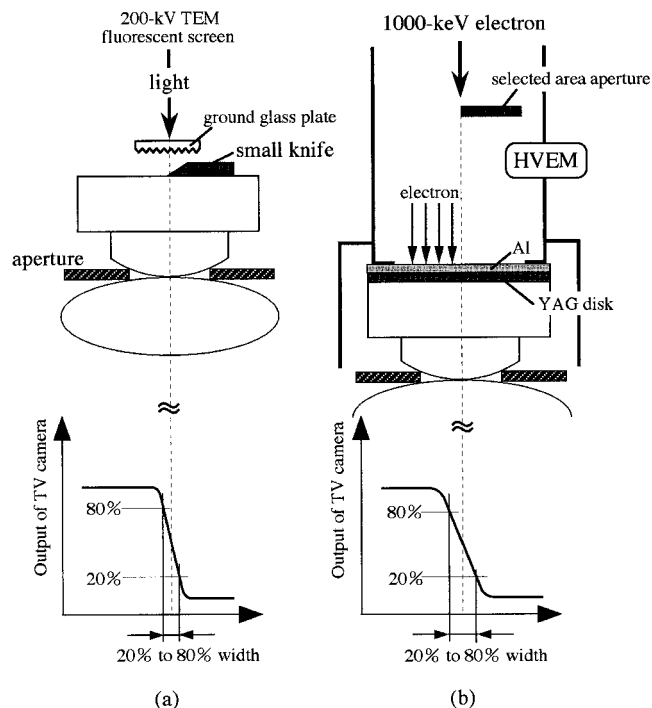


Fig. 5. Experimental setup for measuring resolution. **a:** Light-optical experiment. **b:** 1,000-keV electron beam experiment. The resolution was measured with the edge image of (a) a small knife edge; (b) a selected area aperture.

The overall resolution including the electron beam spread in the YAG disk was measured on an HVEM (Hitachi HU-1000D). The shadow images of a selected area aperture in the HVEM were used as the edge images, as shown in Figure 5b. The measured resolution was 50–60  $\mu\text{m}$  on the YAG disk plane. We found from the experiments that the influence of each part, (1), (2), and (3), on the resolution was about 30  $\mu\text{m}$ . This value for the influence of the electron beam spread in the YAG disk (100- $\mu\text{m}$ -thick) conforms to other studies (Kotera and Kamiya, 1994; Nishi et al., 1996a). Table 1 shows a comparison of the resolution between the new TV system and a conventional P22 fluorescent powder screen and LC TV system. We can observe images magnified 1.35 times compared to the images of the conventional system, because the blurring of the new system is less. Figure 7 shows an example of a 1,000-keV electron microscope image of gold particles on a thin carbon film obtained with the new system.

### Light Intensity

In order to verify the improvement of the light collection efficiency with the glass hemisphere, the light intensity of the new system was compared with that of the system from which the glass hemisphere was removed, and also with that of the conventional system. The output voltage of the TV camera was measured as the light intensity, and the comparison was made after adjusting the magnification of the lens system so that the resolution of each system was the same on the photocathode of the TV camera. Figure 8 shows the

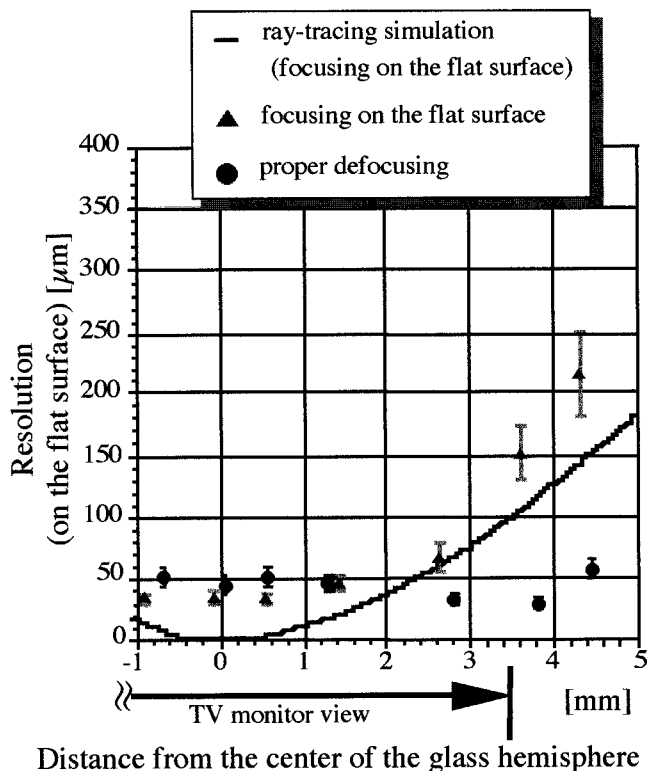


Fig. 6. Resolution depends on the position on the flat surface of the glass hemisphere in the light optical experiment.

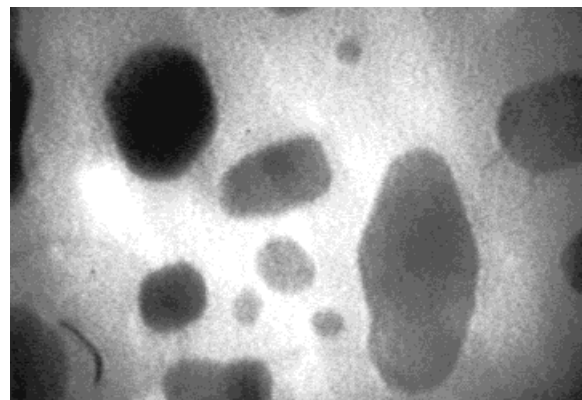
TABLE 1. Resolution of the new TV system and the conventional TV system

LC method TV system	Resolution ( $\mu\text{m}$ )	
	On the screen plane	On the photocathode plane
YAG + glass hemisphere ( $\times 1.35$ )	50–60	70–80
P22 (fluorescent powder screen) ( $\times 1.0$ )	70	70

light intensity of each system as a function of current density on the specimen plane. We verified that the light collection efficiency of the new system with the glass hemisphere improved by a factor of 2.9. We also found that the light intensity of the new system was almost the same as that of the conventional system, although the luminous efficiency of YAG is 1/3 that of P22. This means that the disadvantage of the LC method using the YAG screen has been overcome.

### Shading

Uniformity of the light intensity was measured by exposing a uniform electron beam on the YAG disk of the new system. Figure 9 shows the light intensity distribution as a function of the distance from the center on the disk. Although the light intensity decreases with the distance from the center, the shading factor was below 20% within a circular area having a 3-mm radius at the center, which corresponds to 97% of the



1 [mm]  
(on the YAG disk plane)

Fig. 7. 1,000-kV electron microscope image obtained by the new system. (specimen: gold particles on a thin carbon film).

TV monitor view. The shading, which is due to the glass hemisphere, will not affect TV observation.

### Distortion

Generally, distortion is evaluated by a distortion factor

$$D = (Y - Y_0)/Y_0, \quad (1)$$

where  $Y$  is the distance between the center and a distorted image point and  $Y_0$  is the distance between the center and an ideal image point. A mesh sheet (100- $\mu\text{m}$  spacing) was attached to the glass hemisphere instead of the YAG disk, and the light was illuminated to the new system. Figure 10 shows the image of the mesh sheet. Although a pincushion distortion is observed, the distortion factor  $D$  is small, within 4% at the corners of the TV monitor view. The larger the radius of curvature of the glass hemisphere is, the smaller the distortion. Nevertheless, the measured distortion will not hinder TV observation.

### DQE (Detection Quantum Efficiency)

DQE is an effective factor for analyzing characteristics of a detection system (Herrmann and Krahl, 1984). It is the ratio of the square of the SN ratio of the output signal to that of the input signal, defined as

$$\text{DQE} = \frac{(S/N)_{\text{out}}^2}{(S/N)_{\text{in}}^2} \leq 1. \quad (2)$$

The value of DQE is less than 1, because noise exists in every detection system. An experimental setup for measuring DQE is shown in Figure 11. Electrons of 1,000-keV irradiated uniformly in the new system, and the output voltage of the TV camera was measured by using a digital oscilloscope to obtain the  $(S/N)_{\text{out}}$ . The  $(S/N)_{\text{in}}$  was calculated from the number of incident electrons measured by a Faraday cup. Assuming that the number of incident electrons varies according to the

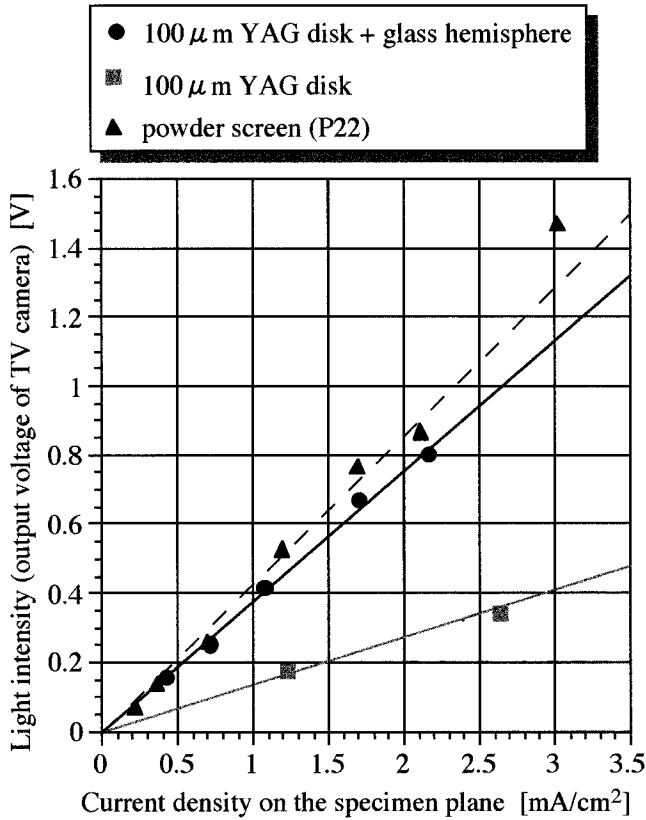


Fig. 8. Comparison of the light intensities of each system. The glass hemisphere improves light collection efficiency, so the light intensity of the new system is almost the same as that of the conventional system (P22 powder screen + LC).

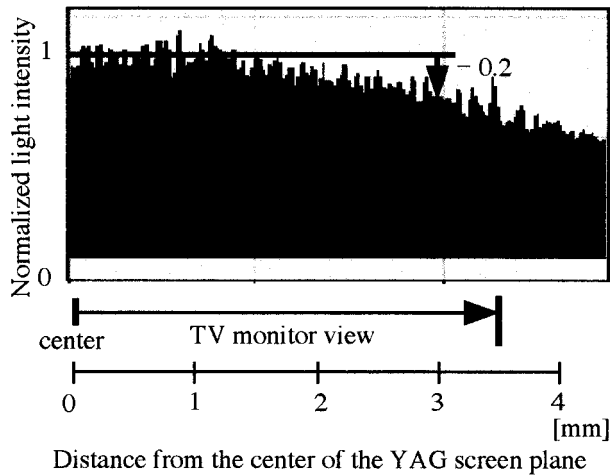


Fig. 9. Uniformity of the light intensity. Light reduction (shading factor) is below 20% within a central circular area having a radius of 3 mm, which corresponds to 97% of the TV monitor view.

probability of a Poisson distribution, we can express  $(S/N)_{in}$  as

$$(S/N)_{in} = \left( \frac{n}{\sqrt{n}} \right) = \sqrt{n}, \quad (3)$$

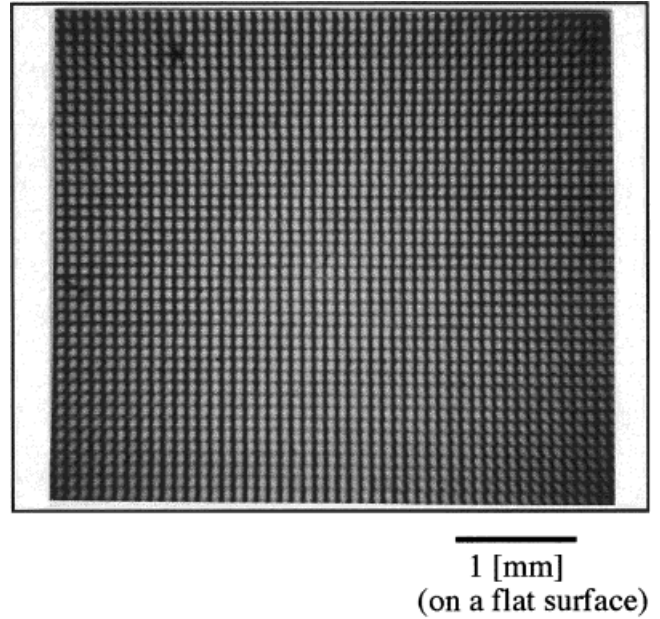


Fig. 10. Image of a mesh sheet (100- $\mu$ m spacing) put on the flat surface of the glass hemisphere. The area surrounded by the outer frame shows the TV monitor view. The distortion factor is 4% at the corners of the TV monitor.

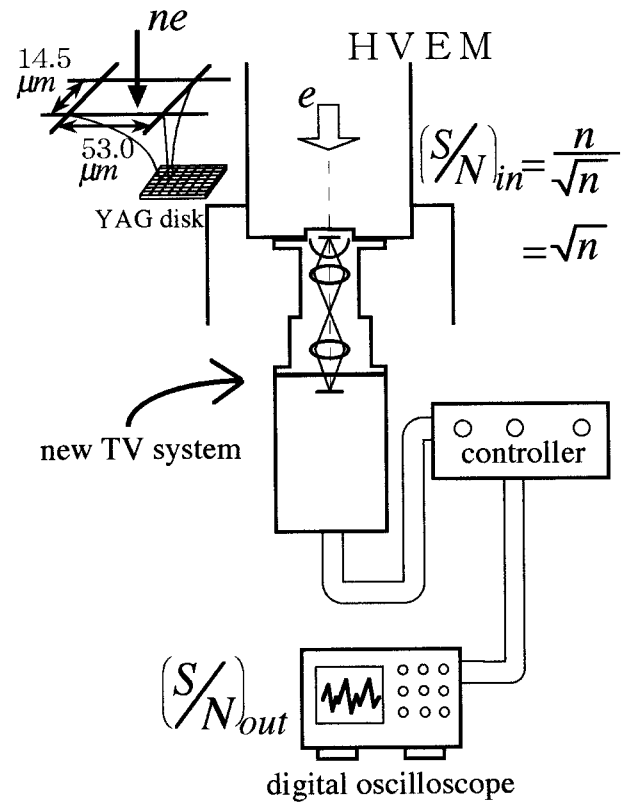


Fig. 11. Experimental setup for DQE measurement. The  $(S/N)_{in}$  is calculated from the number of incident electrons in a pixel. The  $(S/N)_{out}$  is measured from the output voltage of the TV camera.

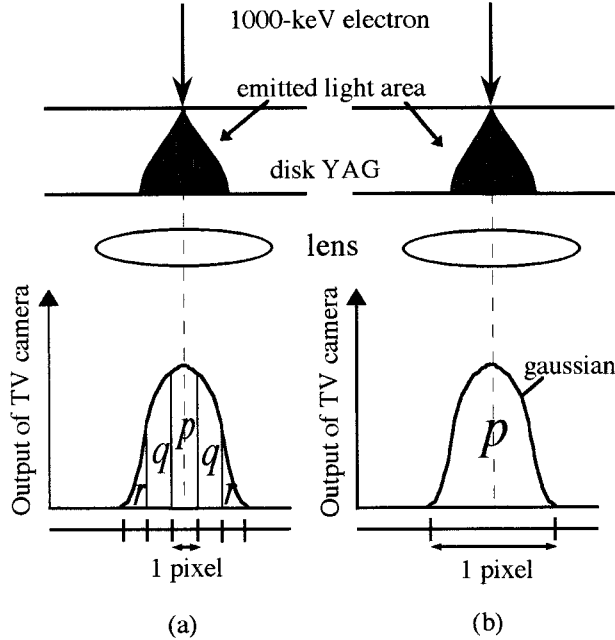


Fig. 12. Influence of the channel mixing effect. **a:** The emitted light and lens aberration influence the output of the neighboring pixels, leading to the overestimation of DQE. **b:** A larger pixel size reduces the effect.

where  $n$  is the average number of incident electrons. We have to take conception of pixels to measure the  $(S/N)_{in}$  and the  $(S/N)_{out}$  of TV systems. Then, we have to take the channel mixing effect into account to calculate DQE. As shown in Figure 12a, the channel mixing effect is caused by the influence of the emitted light, lens aberration, and so forth, on neighboring pixels and overestimating the value of DQE because the output of TV camera is also detected in the neighboring pixels (Ishizuka, 1993). The size of pixels is larger, as shown in Figure 12b, and the measured DQE is closer to the accurate DQE, but the large pixel size lowers the precision of  $S/N$  measurements because the total number of pixels is less. We defined the pixel size as the same as the resolution mentioned in Resolution. The pixel size was defined as  $53.0 \times 14.5 \mu\text{m}$ , as shown in Figure 11. Though the pixel size of the  $x$ -direction can be defined by the resolution, that of the  $y$ -direction is determined by the width of scanning lines. Therefore, the channel mixing effect is more serious in the  $y$ -direction than in the  $x$ -direction. We used the correction method of the channel mixing effect as mentioned in the next paragraph.

First, we have to determine the distribution of the output broadening. The distribution was assumed to be expressed by the Gaussian function. Two-dimensional Gaussian function is

$$f(x, y) = \frac{1}{\sqrt{2\pi}\sigma} \text{Exp} \left[ -\frac{1}{2} \left( \frac{x^2 + y^2}{\sigma^2} \right) \right], \quad (4)$$

where  $\sigma$  is the standard deviation and  $f(x, y)$  satisfies the equation

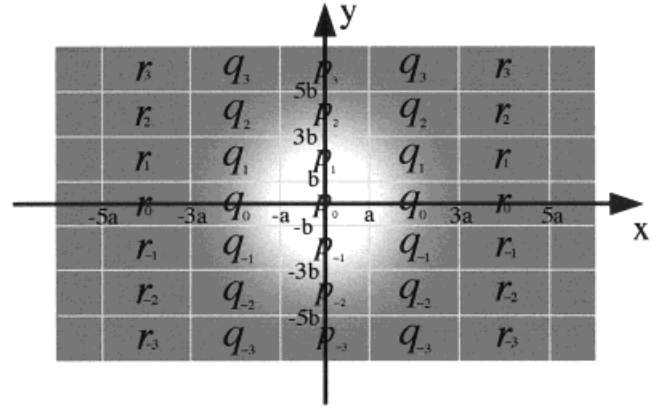


Fig. 13. Illustration of the output distribution on the screen when an electron irradiates the point  $(0, 0)$ .

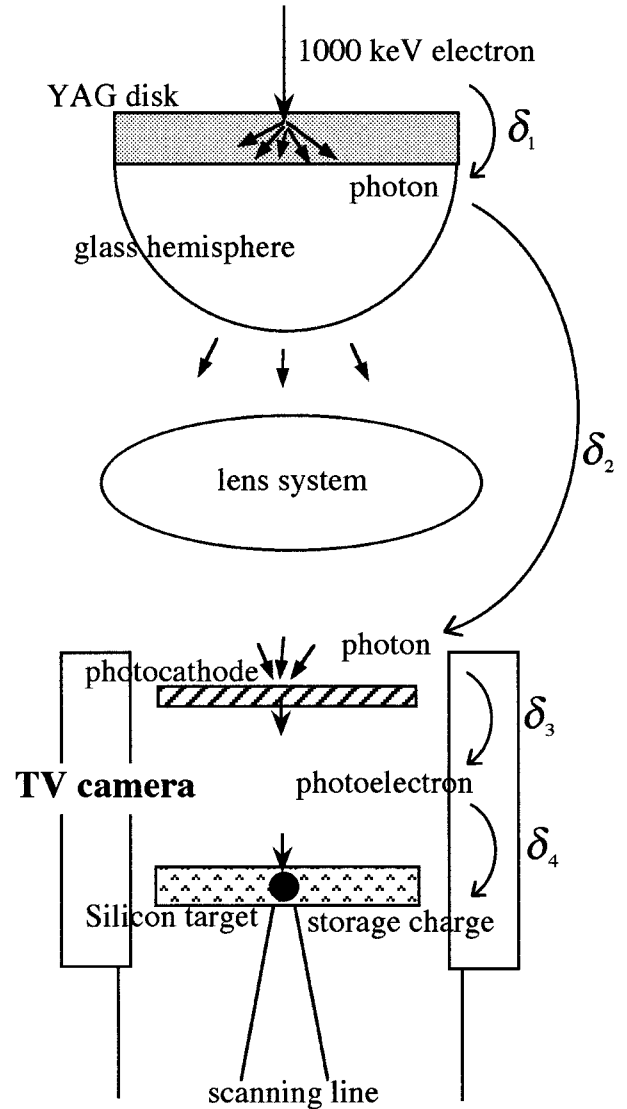


Fig. 14. Schematic diagram of the quantum conversion and the light transferring processes in the new TV system.

$$\int_{-\infty}^{\infty} \int_{-\infty}^{\infty} f(x, y) dx dy = \sqrt{2\pi}\sigma. \quad (5)$$

When an electron irradiates one point ( $x = y = 0$ ), the output distribution on the YAG screen plane is schematically described as shown in Figure 13. The pixel size is  $2a \times 2b$ , and  $p_j, q_j, r_j, \dots$  represent rates of the output in the pixel:

$$\sum_{j=-\infty}^{\infty} p_j + 2 \sum_{j=-\infty}^{\infty} q_j + 2 \sum_{j=-\infty}^{\infty} r_j + \dots = 1. \quad (6)$$

DQE is expressed mathematically by using  $p_j, q_j, r_j, \dots$ . Figure 14 shows the conversion processes between the incident electrons and the output signal of the TV camera. These processes are as follows: ① the incident electrons irradiate the screen (the number of electrons in a pixel:  $n_1$ ), ② the incident electrons convert to photons (conversion efficiency:  $\delta_1$ ), ③ the photons reach the photocathode through the lens system (light transferring efficiency:  $\delta_2$ ), ④ photons reaching the photocathode convert to photoelectrons (conversion efficiency:  $\delta_3$ ), ⑤ the photoelectrons are accelerated by an intensifier and convert to storage electrons in a silicon target of the TV camera (conversion efficiency:  $\delta_4$ ). Assuming that the number of incident electrons, the quantum conversion, and the light transferring in each process vary according to the probability of the Poisson distribution, we can express the noise caused by ① in each pixel as

$$\text{noise in pixel } p_j: \sqrt{n_1} \delta_1 \delta_2 \delta_3 \delta_4 \cdot p_j,$$

$$\text{noise in pixel } q_j: \sqrt{n_1} \delta_1 \delta_2 \delta_3 \delta_4 \cdot q_j,$$

$$\text{noise in pixel } r_j: \sqrt{n_1} \delta_1 \delta_2 \delta_3 \delta_4 \cdot r_j.$$

Similarly, the noise caused by ②–⑤ is written by altering  $\sqrt{n_1} \delta_1 \delta_2 \delta_3 \delta_4$  to  $\sqrt{n_1} \delta_1 \delta_2 \delta_3 \delta_4 - \sqrt{n_1} \delta_1 \delta_2 \delta_3 \delta_4$ , respectively.

Also, we should consider the noise due to the gain fluctuation and read-out noise of the TV camera. The gain fluctuation leads to noise that is proportional to the incident electron density. So, the noise in pixel  $p_j$  is expressed as  $\alpha n_1 \delta_1 \delta_2 \delta_3 \delta_4 \cdot p_j$ , where  $\alpha$  is a proportional constant. The read-out noise ( $Nr$ ) in pixel  $p_j$  is  $Nr \cdot p_j$ .

Since the noises in each pixel are independent of each other, the total noise  $N$  is expressed by the square root of the sum of the squares:

$$\begin{aligned} N &= \sqrt{n_1} \delta_1 \delta_2 \delta_3 \delta_4 \\ &\times \left\{ \left( \sum_{j=-\infty}^{\infty} p_j^2 + 2 \sum_{j=-\infty}^{\infty} q_j^2 + 2 \sum_{j=-\infty}^{\infty} r_j^2 + \dots \right) \right. \\ &\quad \cdot \left( 1 + \frac{1}{\delta_1} + \frac{1}{\delta_1 \delta_2} + \frac{1}{\delta_1 \delta_2 \delta_3} + \frac{1}{\delta_1 \delta_2 \delta_3 \delta_4} \right. \\ &\quad \left. \left. + \alpha^2 n_1 + \frac{Nr^2}{n_1 \delta_1^2 \delta_2^2 \delta_3^2 \delta_4^2} \right) \right\}^{1/2}. \quad (7) \end{aligned}$$

TABLE 2. Parameters of the new TV system

Conversion process	Conversion factor	Value
1,000 keV electron photon	$\delta_1$	3,600
Photon (lens) photon	$\delta_2$	0.015
Photon photoelectron	$\delta_3$	0.10
Photoelectron storage charge	$\delta_4$	4,000
Coefficient of gain fluctuation noise	$\alpha$	0.168
Read-out noise (the number of storage charges)	$Nr$	$1.3 \times 10^5$

The value of each parameter ( $\delta_1$ – $\delta_4$ ,  $\alpha$ ,  $Nr$ ) was estimated by simple experiments for our TV system and earlier studies (Guldberg and Schroder, 1971; Miyashiro and Shirouzu, 1971; Nishi et al., 1996a,b), as shown in Table 2. We found that the noise caused by ①, ④, the gain fluctuation, and the read-out have a greater impact on the total noise  $N$ . Therefore, the total noise  $N$  can be approximated by

$$\begin{aligned} N &\cong \sqrt{n_1} \delta_1 \delta_2 \delta_3 \delta_4 \\ &\times \left\{ \left( \sum_{j=-\infty}^{\infty} p_j^2 + 2 \sum_{j=-\infty}^{\infty} q_j^2 + 2 \sum_{j=-\infty}^{\infty} r_j^2 + \dots \right) \right. \\ &\quad \cdot \left( 1 + \frac{1}{\delta_1 \delta_2 \delta_3} + \alpha^2 n_1 + \frac{Nr^2}{n_1 \delta_1^2 \delta_2^2 \delta_3^2 \delta_4^2} \right) \left. \right\}^{1/2}. \quad (8) \end{aligned}$$

From the output signal ( $n_1 \delta_1 \delta_2 \delta_3 \delta_4$ ) and Eq. (3), DQE is expressed as

$$\begin{aligned} \text{DQE} &= \frac{(S/N)_{\text{out}}^2}{(S/N)_{\text{in}}^2} = \\ &\left\{ \left( \sum_{j=-\infty}^{\infty} p_j^2 + 2 \sum_{j=-\infty}^{\infty} q_j^2 + 2 \sum_{j=-\infty}^{\infty} r_j^2 + \dots \right) \right. \\ &\quad \cdot \left( 1 + \delta_1 \delta_2 \delta_3 + \alpha^2 n_1 + \frac{Nr^2}{n_1 \delta_1^2 \delta_2^2 \delta_3^2 \delta_4^2} \right) \left. \right\}^{-1}. \quad (9) \end{aligned}$$

If the channel mixing effect does not exist,  $p_0 = 1$  and other rates  $p_j, q_j, r_j, \dots$  ( $p_j \neq p_0$ ) are equal to 0, the corrected DQE (DQECor) is

$$\begin{aligned} \text{DQECor} &= \frac{(S/N)_{\text{out}}^2}{(S/N)_{\text{in}}^2} \\ &= \left( 1 + \frac{1}{\delta_1 \delta_2 \delta_3} + \alpha^2 n_1 + \frac{Nr^2}{n_1 \delta_1^2 \delta_2^2 \delta_3^2 \delta_4^2} \right)^{-1}. \quad (10) \end{aligned}$$

In order to obtain the DQECor, the measured DQE is multiplied by a correction factor

$$Cc = \left( \sum_{j=-\infty}^{\infty} p_j^2 + 2 \sum_{j=-\infty}^{\infty} q_j^2 + 2 \sum_{j=-\infty}^{\infty} r_j^2 + \dots \right). \quad (11)$$

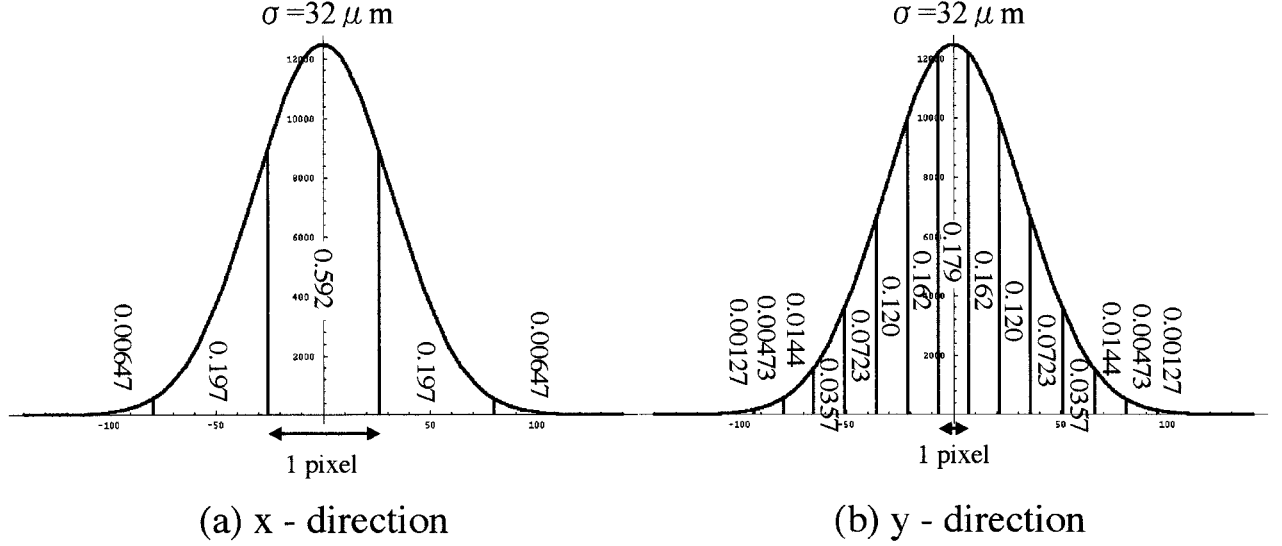


Fig. 15. Experimental rates of the output in neighboring pixels of (a)  $x$ -direction, (b)  $y$ -direction.

The correction factor  $C_c$  is expanded analytically by using Eqs. (4) and (5) on Figure 13. First term in Eq. (11) is expressed by

$$\sum_{j=-\infty}^{\infty} p_j^2 = \left( \frac{1}{\sqrt{2\pi}\sigma} \right)^4 \left\{ \int_{-a}^a \text{Exp} \left( -\frac{1}{2} \cdot \frac{x^2}{\sigma^2} \right) dx \right\}^2 \cdot \sum_{j=-\infty}^{\infty} \left[ \left\{ \int_{(2j-1)b}^{(2j+1)b} \text{Exp} \left( -\frac{1}{2} \cdot \frac{y^2}{\sigma^2} \right) dy \right\}^2 \right].$$

The terms of  $q_j$ ,  $r_j$ , ... are written in the similar way. As a result, we obtain

$$C_c = \sum_{i=-\infty}^{\infty} \left[ \left\{ \frac{1}{\sqrt{2\pi}\sigma} \int_{(2i-1)a}^{(2i+1)a} \text{Exp} \left( -\frac{1}{2} \cdot \frac{x^2}{\sigma^2} \right) dx \right\}^2 \right] \cdot \sum_{j=-\infty}^{\infty} \left[ \left\{ \frac{1}{\sqrt{2\pi}\sigma} \int_{(2j-1)b}^{(2j+1)b} \text{Exp} \left( -\frac{1}{2} \cdot \frac{y^2}{\sigma^2} \right) dy \right\}^2 \right]. \quad (12)$$

The sigma terms correspond to the sums of the contributions to each pixel according to one-dimensional Gaussian distributions in the  $x$ -direction and the  $y$ -direction, respectively.

The output distribution  $I(x)$  due to the small edge mentioned in Resolution is expressed by using Eq. (4) as follows:

$$I(x) = \int_{X=-\infty}^{X=x} \int_{Y=-\infty}^{Y=\infty} f(X, Y) dXdY, \quad (13)$$

The 20–80% width of the profile given by this equation corresponds to  $1.7\sigma$ . In our experiment, the output

broadening was expressed as a Gaussian distribution of  $\sigma = 32 \mu\text{m}$  ( $55 \mu\text{m}/1.7$ ). The rates  $p_j$ ,  $q_j$ ,  $r_j$ , ... were calculated as Figure 15a and b and the correction factor  $C_c = 0.0544$ . Figure 16 shows the  $\text{DQE}_{\text{cor}}$  as a function of the incident electron density (or the number of incident electrons) on the YAG disk plane. The fitted curve is derived by Eq. (10) and the values given in Table 2. The  $\text{DQE}_{\text{cor}}$  decreases as the incident electron density increases. This is why the noise, which is proportional to the incident electron density, affects  $\text{DQE}_{\text{cor}}$ . It seems to be the noise caused by the gain fluctuation of the TV camera. In usual TV observations, the incident electron density used for observation is around  $200 \text{ pA}/\text{cm}^2$ , corresponding to  $\text{DQE}_{\text{cor}}$  of about 0.1. The DQE of the detector for 100–200 kV TEM is around 0.7 (Daberkow et al., 1991; Fan and Ellisman, 1993; Zuo, 1996). For the HVEM detector, however, DQEs reported so far were about 0.1. For example, the DQE of the photographic film for 1,000 kV is 0.15 to 0.25 (Kamiya and Aarii, 1990), that of the parallel detector of electron energy loss spectrum for 500 kV is 0.10 (Yoshida et al., 1991), and that of the imaging plate for 1,250 kV is 0.05 (Taniyama et al., 1997). Therefore, the value of  $\text{DQE}_{\text{cor}}$  of our new TV system is reasonable for HVEM.

## CONCLUSIONS

A new lens coupling TV system for HVEM using a YAG disk screen and a glass hemisphere has been developed. The performance of the system is summarized as follows.

1. Resolution: The blurring of electron microscope images was caused by the electron beam spread in the YAG disk, the curvature of image field due to the glass hemisphere, and the misalignment of the lens system. The resolution was about  $55 \mu\text{m}$  on the screen plane. The new system has 1.3 times higher resolution than the conventional system.

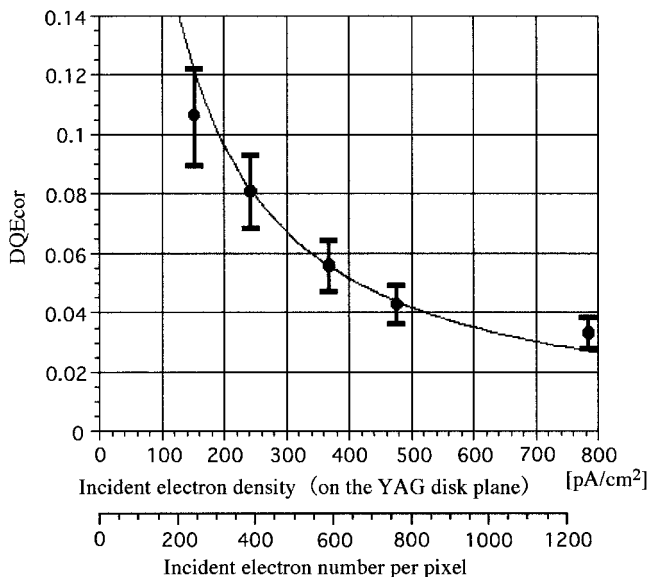


Fig. 16. DQE corrected for the channel mixing effect.

2. Light intensity: Light intensity was improved to the same value as that of the conventional P22 powder screen and LC system, although the luminous efficiency of YAG is  $\frac{1}{3}$  that of P22.
3. Shading: Uniformity of light intensity was within 80% for the TV monitor view.
4. Distortion: The distortion factor was within 4% at the corners of the TV monitor view.
5. DQE: The detection quantum efficiency (DQE), after correcting for the channel mixing effect, is about 0.1.

The new HVEM TV system, which performs sufficiently well for TV observation and reduces the amount of damage caused by high-energy electron irradiation and the influence of X-rays, has been made possible by the new lens coupling method using a YAG disk and glass hemisphere.

#### ACKNOWLEDGMENTS

We thank Mr. Chiaki Morita and Mr. Shigeo Arai for their help with the HU-1000D high voltage electron microscope. We are also grateful to Dr. Shigeyasu Tanaka, Dr. Takaaki Hanai, and Mr. Kenji Ban for their many valuable suggestions regarding the design

and the construction of the new lens system with the glass hemisphere.

#### REFERENCES

- Autrata R, Schauer P, Kvapil Jos, Kvapil J. 1983. Single-crystal aluminates—A new generation of scintillators for scanning electron microscopes and transparent screens in electron optical devices. *Scan Electr Microsc II*:489–500.
- Ayato H, Mori N, Miyahara J, Oikawa T. 1990. Application of the Imaging Plate to TEM Observation. *J Electron Microsc 39*:444–448.
- Barbe DF, editor. 1980. Charge-coupled devices, Vol. 38. New York: Springer-Verlag.
- Daberkow I, Herrmann K-H, Liu Libin, Rau WD. 1991. Performance of electron image converters with YAG single-crystal screen and CCD sensor. *Ultramicroscopy 38*:215–223.
- Fan GY, Ellisman MH. 1993. High-sensitivity lens-coupled slow-scan CCD camera for transmission electron microscopy. *Ultramicroscopy 52*:21–29.
- Guldberg J, Schroder DK. 1971. Theoretical and experimental gain of electron-excited silicon targets. *IEEE Transactions on Electron Devices*, Vol. ED-18, No. 11, November, p 1029–1035.
- Herrmann K-H, Krahl D. 1984. Electronic image recording in conventional electron microscopy. In: Barer R, Cosslett VE, editors. *Advances in optical and electron microscopy*, Vol. 9. New York: Academic Press.
- Ishizuka K. 1993. Analysis of electron image detection efficiency of slow-scan CCD cameras. *Ultramicroscopy 52*:7–20.
- Kamiya Y, Arai T. 1990. Granularity noise of photographic emulsions: accuracy of intensity measurement by photographic films. *J Electr Microsc 39*:351–355.
- Kotera M, Kamiya Y. 1994. Computer simulation of light emission by high-energy electrons in YAG single crystals. *Ultramicroscopy 54*:293–300.
- Krivanek OL, Mooney PE. 1993. Applications of slow-scan CCD cameras in transmission electron microscopy. *Ultramicroscopy 49*:95–108.
- Miyashiro S, Shirouzu S. 1971. Silicon electron multiplication (SEM) camera tube. *IEEE Transactions on Electron Devices*, Vol. ED-18, No. 11, November, p 1023–1028.
- Mooney PE, Bui DN, Krivanek OL. 1994. Design of a slow scan CCD camera for 1 MV operation. *ICEM 13-PARIS 17–22*.
- Mori N, Oikawa T, Harada Y, Miyahara J. 1990. Development of the imaging plate for the transmission electron microscope and its characteristics. *J Electr Microsc 39*:433–436.
- Nishi R, Yoshida K, Takaoka A, Katsuta T. 1996a. Electron energy dependence of characteristics of fluorescent plates for ultrahigh-voltage electron microscopes. *Ultramicroscopy 62*:271–275.
- Nishi R, Yoshida K, Takaoka A. 1996b. Measurement of luminous broadening with sandwich-structure fluorescent plates. *J Electr Microsc 45*:148–151.
- Taniyama A, Shindo D, Oikawa T. 1997. Detective quantum efficiency of the 25  $\mu\text{m}$  pixel size imaging plate for transmission electron microscopes. *J Electr Microsc 46*:303–310.
- Weickenmeier AL, Nuchter W, Mayer J. 1995. Quantitative characterization of point spread function and detection quantum efficiency for a YAG scintillator slow scan CCD camera. *Optik 99*:147–154.
- Yoshida K, Takaoka A, Ura K. 1991. Channel mixing effect on SN-ratio of electron energy loss spectrum in parallel detector. *J Electr Microsc 40*:319–324.
- Zuo JM. 1996. Electron detection characteristics of slow-scan CCD camera. *Ultramicroscopy 66*:21–33.